Mon. Not. R. astr. Soc. (1976) **177**, 625–643.

INFRARED PHOTOMETRY, EXTINCTION CURVES AND *R* VALUES FOR STARS IN THE SOUTHERN MILKY WAY

*D. C. B. Whittet**, *I. G. van Breda**†

University Observatory, St Andrews, Fife

and I. S. Glass

South African Astronomical Observatory, PO Box 9, Observatory, Cape 7935, South Africa

(Communicated by the Director, University Observatory, St Andrews)

(Received 1976 June 7)

SUMMARY

Infrared photometry in the *JHKL* bands is combined with photoelectric scanner photometry to give interstellar extinction curves in the range λ 0·34–3·4 μ for 22 early-type stars in the Southern Milky Way. The extinction curves show variations in curvature in the infrared which are related to the well-known change in slope in the near ultraviolet. The curves are extrapolated to $\lambda^{-1} = 0$ with the aid of Mie theory computations for a graphite–iron–silicate grain model, and values of the ratio of total to selective extinction $R = A_V/E_{B-V}$ are deduced. *R* is found to vary between 2·7 and 3·5 with a median value of 3·2 for stars with long-path-length reddening, while two stars in the ρ Ophiuchi dark cloud have *R* values of 3·6 and 4·3. The variations found in the extinction curves probably result from regional fluctuations in the mean grain size and/or composition along the line of sight, and any systematic variation in *R* with galactic longitude is likely to be small. The derived *R* values are correlated with the wavelength of maximum polarization. *R* is found to be normal for HD 90706 in the cluster IC 2581, for which a high *R* value has been suggested. We note that *R* has now been shown to lie in the range 4·1–4·4 for stars in the denser regions of the ρ Ophiuchi cloud by four independent methods.

None of the observed stars show strong infrared excess radiation at 3·4 μ. Small excesses measured for a few high-luminosity stars associated with mass loss may be due to free–free emission in gaseous stellar envelopes.

1. INTRODUCTION

In an earlier paper (Whittet, van Breda & Nandy 1973, hereafter referred to as Paper I) optical scanner observations were reported for a set of 22 reddened stars distributed along the Southern Milky Way. These were made on the 36-in telescope of the Cerro Tololo Interamerican Observatory, Chile, and the data used to derive interstellar extinction curves by the colour difference method in

* Visiting astronomers, Cerro Tololo Interamerican Observatory, which is operated by the Association of Universities for Research in Astronomy, Inc., under contract with the National Science Foundation.

† Present address: Royal Greenwich Observatory, Herstmonceux, Sussex.

the range λ 3480–8040. Results showed that there is appreciable variation from star to star in the slope of the ultraviolet section of the normalized extinction curves beyond the change in slope or 'knee' which occurs in the λ 4200–4600 region. These variations are not apparently related to position in the galactic plane, and there are cases where stars quite close together in the sky show significantly different curves. The stars were divided into groups according to the magnitude of the change in slope, and these were labelled A, B, . . . , F in order of decreasing ultraviolet slope. In order to assess the effect, if any, of these variations on estimates of the total absorptions and hence the photometric distances of the stars, the wavelength coverage has been extended into the infrared by means of photometry in the J, H, K and L bands (effective wavelengths 1·25, 1·65, 2·2 and 3·4 μ). Data for two of the reddened stars, HD 92964 (extinction law D), HD 147889 (originally classified C) and a comparison star were reported by van Breda, Glass & Whittet (1974, hereafter Paper II). In that paper the extinction curves were extrapolated graphically to $\lambda^{-1} = 0$ in order to give values of the ratio of total to selective extinction $R = A_V/E_{B-V}$. A possible downward trend in each curve at the L (3·4 μ) wavelength was ignored in making the extrapolation because of the possibility of contamination by infrared excess emission from the reddened star, the photometric errors being in any case large at this wavelength due to the faintness of the comparison star. The possibility of infrared radiation distorting the extinction curves is one of the principal objections that has been raised to the high R values quoted by Johnson (1968). This paper presents infrared photometry for the remaining 20 reddened stars listed in Paper I and associated comparison stars. New scanner data is also presented for one of the reddened

TABLE I

Broadband photometric data for 20 reddened stars

HD	V	$B-V$	$U-B$	J	H	K	L
77581	(6·87)	0·50	−0·49	5·85	5·71	5·60	5·56
90706	7·07	0·47	−0·43	5·97	5·80	5·69	5·84
115842	6·02	0·29	−0·72	5·33	5·23	5·15	5·11
142468	7·85	0·58	−0·38	6·60	6·44	6·32	6·19
144969	8·28	0·94	−0·08	5·92	5·58	5·36	5·13
147084	4·55	0·83	(0·63)	2·23	1·85	1·62	1·45
148379	5·34	(0·56)	−0·56	4·01	3·81	3·67	3·55
148688	5·32	0·34	−0·75	4·36	4·23	4·11	4·03
152235	6·30	0·51	−0·45	4·99	4·83	4·72	4·61
152236	4·73	(0·50)	(−0·58)	3·47	3·27	3·11	2·94
154043	7·09	0·63	−0·38	5·54	5·36	5·21	5·12
156201	7·90	0·65	−0·37	6·30	6·08	5·95	5·86
165319	7·94	0·59	−0·50	6·53	6·35	6·27	6·21
166628	7·17	0·57	−0·29	5·75	5·54	5·41	5·38
167838	6·73	0·46	−0·36	5·54	5·37	5·27	5·20
168571	7·79	0·53	−0·40	6·46	6·23	6·07	6·11
169454	6·61	0·94	−0·18	4·42	4·08	3·85	3·69
170938	7·87	0·85	−0·25	5·76	5·47	5·29	5·12
171012	6·82	0·45	−0·57	5·78	5·67	5·54	5·40
172488	7·62	0·54	−0·40	6·49	6·39	6·28	6·31

Note:
(Parentheses indicate a spread of ±0·05 or more in published UBV photometry about the mean given.)

stars, HD 147084, with an alternative comparison star giving a better spectral type match than that used in Paper I. A model-fitting process is applied to the derived extinction curves in order to provide a theoretical basis for extrapolation to $\lambda^{-1} = 0$. The results are used to deduce R values, total absorptions and photometric distances for the individual reddened stars.

2. INFRARED PHOTOMETRY AND EXTINCTION CURVES

The infrared observations were made in 1974 April, using the photometer constructed by Glass (1973), on the 1·02-m telescope at the Sutherland site of the South African Astronomical Observatory. Standard stars were taken from the list of Glass (1974). The *JHKL* magnitudes are given in Table I (reddened stars) and Table II (comparison stars) along with *UBV* photometry. The standard photometric error is within $0^m{\cdot}03$ at J, H and K in Tables I and II. At L the standard error is within $0^m{\cdot}05$ up to $L = 5{\cdot}0$, rising to $0^m{\cdot}10$ at $L = 6{\cdot}0$ and $0^m{\cdot}20$ at $L = 6{\cdot}8$. The infrared results for HD 214080 (Table II) were not measured directly as the star is inaccessible in April; an alternative comparison star, HD 91316 which has identical spectral type (B1Ib) and reddening ($E_{B-V} = 0{\cdot}05$) was observed in order to deduce the expected infrared colours for HD 214080. The pairing of reddened and comparison stars is given in Table III, in which the reddened stars are divided into groups according to the classification of their extinction curves. The stars HD 92964 and HD 147889 for which infrared data were reported in Paper II are included in Table III. The *UBV* photometry in Tables I and II and the MK spectral types in Table III are compiled variously from Jaschek, Conde & de Sierra (1964), Blanco *et al.* (1968), Cousins (1973) and Kennedy & Buscombe (1974). Fig. 1 shows a composite diagram of the superposed normalized extinction curves for each group. The normalization is such that

$$\Delta m = 1{\cdot}0 \text{ at } \lambda^{-1} = 2{\cdot}193\ \mu^{-1}$$

$$\Delta m = 0{\cdot}0 \text{ at } \lambda^{-1} = 1{\cdot}282\ \mu^{-1}.$$

We note that the ultraviolet slope correlates inversely with the mean infrared slope for groups A, B, C and D. The curve for HD 147889 (labelled C′) is an exception, approximating to curve C in the ultraviolet, but dipping much lower

TABLE II

Broadband photometric data for comparison stars

HD	V	$B-V$	$U-B$	J	H	K	L
64760	4·24	−0·15	−0·99	4·59	4·69	4·74	4·79
74272	4·76	+0·12	+0·12	4·24	4·15	4·10	4·09
91316	3·85	−0·14	−0·96	4·18	4·22	4·26	4·27
99171	6·11	−0·19	−0·80	6·48	6·60	6·65	6·83
136664	4·53	−0·15	−0·62	4·87	4·93	4·97	5·03
148703	4·23	−0·17	−0·80	4·54	4·64	4·68	4·82
150898	5·57	−0·09	−1·02	5·68	5·74	5·77	5·77
166197	6·14	−0·15	−0·85	6·41	6·47	6·50	6·57
172910	4·87	−0·18	−0·71	5·20	5·27	5·31	5·40
214080	6·82	−0·14	−0·91	7·16	7·20	7·24	7·25

Note:
JHKL results for HD 214080 are deduced using those for HD 91316.

TABLE III

Pairs of reddened and comparison stars grouped according to classification of extinction curve

Curve	Reddened Star HD	Reddened Star Sp	Comparison Star HD	Comparison Star Sp
A	172488	B0·5II	214080	B1Ib
B	90706	B3Ib	96088	B3III
	152235	B0·5Ia	150898	B0Iab
	154043	B1Ik }	214080	B1Ib
	156201	B0·5Ia }		
	165319	B0Ia	150898	B0Iab
	166628	B3Ia	172910	B3V
C	77581	B0·5Ib	64760	B0·5Ib
	142468	B0·5Ia	99171	B2IV–V
	144969	B0·5Ia	150898	B0Iab
	147084	A5II	74272	A5II
	148379	B2Ia	166197	B2III
	167838	B5Ia	136664	B5V
	168571	B1II+ }		
	169454	B1Ia }	214080	B1Ib
	170938	B1Ia }		
D	92964	B3Ia	96088	B3III
	115842	B0·5Iab	64760	B0·5Ib
	148688	B1Ia+ }		
	152236	B1Ia }	214080	B1Ib
	171012	B0·5Ia }		
C′	147889	B2V	148703	B2IV

than any of the other curves in the infrared. The comparison star for HD 147889 is HD 148703, not HD 96088 as used in Paper II, being the only one with available infrared data at that time; the extinction curve is almost identical except that the photometric errors are reduced. It must be emphasized that the classification of the curves in groups A–D is not unique; we have averaged together curves of similar overall characteristics, but no two curves are identical. The differences between adjacent mean curves in Fig. 1 are larger than the photometric uncertainties in the plotted points. The grouping of the stars given here is not identical to that reported in Paper I. No significant difference was found between curves D and E when the infrared data was considered. A revised MK classification was adopted for the comparison star HD 99171: B2III/IV–V (Kennedy & Buscombe 1974) gave results more consistent with other comparison stars than B0III (Blanco *et al.* 1968, as used in Paper I) when Balmer discontinuity corrections were applied. As a result, HD 77581 and HD 142468 have been assigned to group C instead of group D because of the slightly increased extinction in the ultraviolet. In the case of HD 77581 another comparison star, HD 64760, also scanned in 1972 but not previously reported, has been used as it gives a better spectral-type match.

The A5II star HD 147084 was previously compared with HD 146145, classified A5 and A7V by references in the Blanco *et al.* catalogue; the resultant curve showed a large peak in the region of the Balmer discontinuity as noted in Paper I.

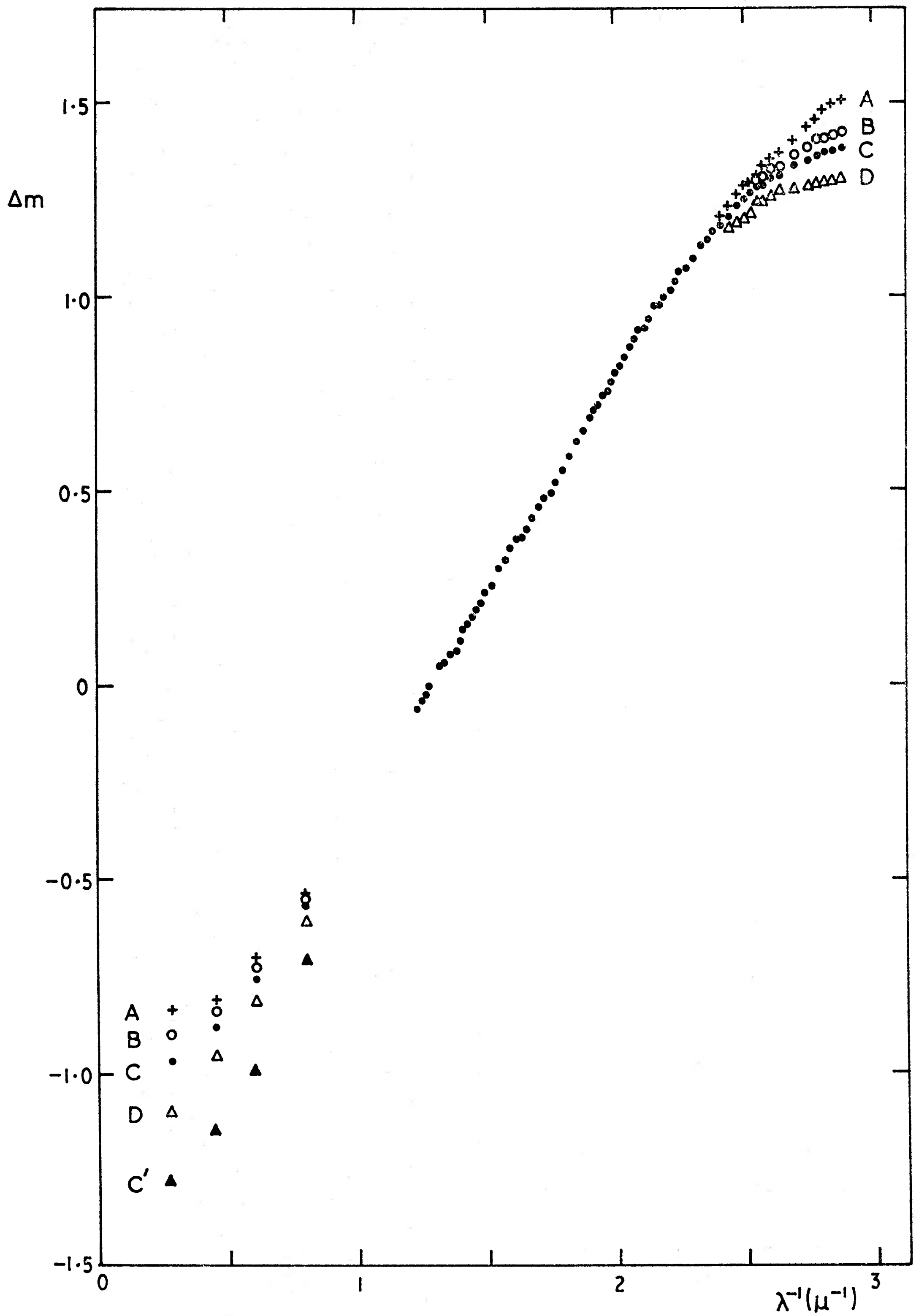

Fig. 1. *Superposed mean extinction curves for the groups in Table III.*

The curve was highly flattened on the long wavelength side of the discontinuity. The star was rescanned at Cerro Tololo in 1974 May, using another comparison star, HD 74272, which has been classified A5II by two references in the catalogue. The scanner extinction curve obtained is compared with that using the original

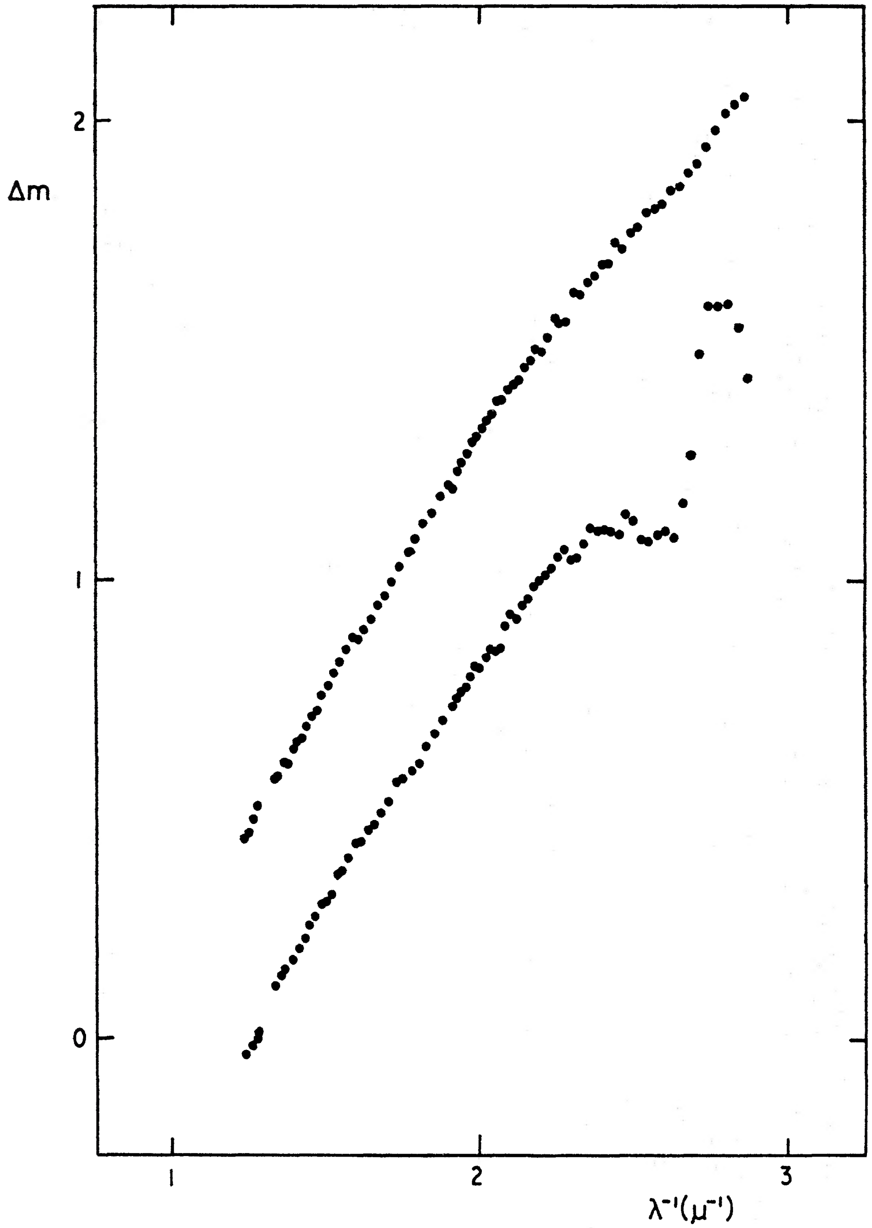

FIG. 2. *Scanner extinction curves for HD* 147084 *compared with HD* 74272 (*upper curve,* 1974 *data*) *and HD* 146145 (*lower curve,* 1972 *data*).

comparison in Fig. 2. A slight upward trend appears beyond the Balmer limit in the upper curve, but there is no hump, confirming that HD 74272 is a better spectral type match. The apparent flattening of the lower curve in the 4500–3800 Å region (2·2–2·6 μ^{-1}) is probably caused by mismatching in the closely spaced Balmer lines. There is also a discrepancy in the infrared, and only in the visual (8000–4500 Å) region do the two curves concur. The extinction curve of HD 147084 has thus been reclassified: it appears to approximate to law C, disregarding the points beyond the Balmer limit. Fig. 2 illustrates the importance of accurately matching star pairs as late as A5. The problem is far less acute for early B-type stars.

The method of correcting for mismatching at the Balmer discontinuity has been described by Divan (1971). Corrections are also applied where necessary for individual Balmer lines using measured equivalent widths. When a Balmer line falls entirely within a spectral element of width $\Delta\lambda$ the required correction to the (unnormalized) extinction Δm is

$$C = 2{\cdot}5 \log \frac{\Delta\lambda - w_{\mathrm{r}}}{\Delta\lambda - w_{\mathrm{c}}}$$

where w_{r} and w_{c} are the equivalent widths for the reddened and comparison stars. When a line overlaps two spectral elements these are considered together and the correction for the combined band width applied to the mean Δm value. Balmer line equivalent widths as a function of MK types have been tabulated by Buscombe (1969).

3. MODEL FITTING

It has been shown in recent years that a three-component grain model is necessary to explain the λ-dependence of the extinction and albedo over the whole of the spectrum now accessible, using currently available optical data for likely solids in Mie theory computations (see Wickramasinghe & Nandy 1970, 1971; Aannestad & Purcell 1973; Greenberg 1973; Wickramasinghe 1974). No unique model has evolved for the grains, however, and its precise composition is still unknown. Graphite grains of radii 0·01–0·05 μ are generally regarded as a probable component due to the correspondence of the π electron transition around λ 2200 to the 'hump' in the extinction curve. The absorption feature around 10 μ seen in the spectra of certain highly obscured stars has been widely attributed to silicate dust, although polymerized formaldehyde has also been put forward as an alternative source of this feature (Wickramasinghe 1974, 1975; Whittet *et al.* 1976). A graphite–iron–silicate model of the form proposed by Wickramasinghe & Nandy (1971, hereafter WN) is adopted for the purposes of the present work. The extinction curves computed by WN are in reasonable agreement with the observations of Bless & Savage (1972). Nandy & Wickramasinghe (1971) showed that the anomalous extinction curves reported for stars in the Orion Nebula can be matched by suitable manipulation of the grain-size distribution. As we are not concerned here with wavelengths below 3480 Å the model-fitting procedure is relatively straightforward.

The Mie theory gives the cross section for extinction of a spherical grain in terms of the Mie coefficients a_{n} and b_{n}:

$$C_{\mathrm{ext}} = \frac{\lambda^2}{2\pi} \sum_{n=1}^{\infty} (2n+1)\, \mathrm{Re}\,(a_{\mathrm{n}} + b_{\mathrm{n}}).$$

These coefficients are defined in terms of Riccati–Bessel functions (see, e.g. Wickramasinghe 1967) and depend on the wavelength λ, the grain radius r and the complex refractive index of the grain material. If we consider a distribution function $n(r)$ for the grain radii, then the extinction is given by

$$\Delta m = 1{\cdot}086 \int_0^{\infty} C_{\mathrm{ext}}\, n(r)\, dr.$$

Theoretical curves were derived using the computational method described by WN, and normalized to allow direct comparison with the observational curves in Fig. 1. The λ dependence of the real and imaginary parts of the refractive index (usually called the optical constants) were taken from Taft & Philipp (1965) and

Lenham & Treherne (1966) as in WN for the graphite and iron components. In the case of silicates, experimentally determined values for obsidian given by Pollack, Toon & Khare (1973) were substituted for the constant real index assumed by WN. There are five input parameters in addition to the optical constants to which values must be assigned to compute a particular curve. These are the radius of maximum frequency or characteristic radius, r_m, for each of the three grain species in the distribution function used:

$$n(r) \propto r^{3/2} \exp\left[-\frac{1}{2}\left(\frac{r}{r_m}\right)^3\right],$$

and the relative weights x_{gr} and x_{ir} of the graphite and iron extinction relative to the silicate extinction measured at λ 4560. Best fits to the data were generally obtained using r_m values in the limits 0·03–0·06 μ for graphite, 0·01–0·04 μ for iron, and 0·20–0·24 μ for silicates. Results are presented here using r_m values of 0·045, 0·025 and 0·22 μ, which give satisfactory results for the observational curves A, B, C and D. Fits to the individual curves were achieved by adjusting the weights x_{gr} and x_{ir}: values which produce a family of curves exhibiting the general trend in the observational extinction A–D (i.e. progressive flattening in the ultraviolet accompanied by increasing downward curvature in the infrared) were found to follow a linear relationship:

$$5\,x_{ir} = x_{gr} + 0{\cdot}5$$

Varying x_{gr} in the range 2·1–0·7 produced curves which gave good fits to laws A, B, C and D in Fig. 1. In the case of curve C′ (HD 147889) it was not possible to fit the ultraviolet and infrared sections simultaneously or to match the general curvature of the data points in the visual region (see Paper II) using this set of r_m values. An increase in the value of r_m for silicates from 0·22 to 0·26 μ was found to produce the required downward trend of curve C′ compared with curve C in the infrared. The values of x_{gr}, x_{ir} and r_m (silicate) for the fits to each mean observational curve are listed in Table IV, and the matching of the theoretical results (continuous curves) with the data is illustrated in Fig. 3 (curves A, B, C and D). For clarity of presentation the curves are separated by $0^m{\cdot}2$ in Fig. 3, the Δm scale applying to curve A. In the case of HD 147889 (Fig. 4) the curve C model is shown as well as the curve C′ model in the infrared to illustrate the effect of increasing r_m. The two curves are very similar in the ultraviolet. It is emphasized that other combinations of the model parameters within the given limits for r_m can give similar results, and the values listed in Table IV are not therefore unique.

Table IV

Values of the parameters x_{gr}, x_{ir} and r_m (sil) for the best fits to each mean observational curve, and the deduced value of R. [$r_m(gr)$ = 0·045 μ and $r_m(ir)$ = 0·025 μ in each case]

Curve	x_{gr}	x_{ir}	r_m (sil) μ	R (±0·2)
A	2·10	0·52	0·22	2·7
B	1·25	0·35	0·22	3·0
C	0·90	0·28	0·22	3·3
D	0·70	0·24	0·22	3·5
C′	1·00	0·30	0·26	4·3

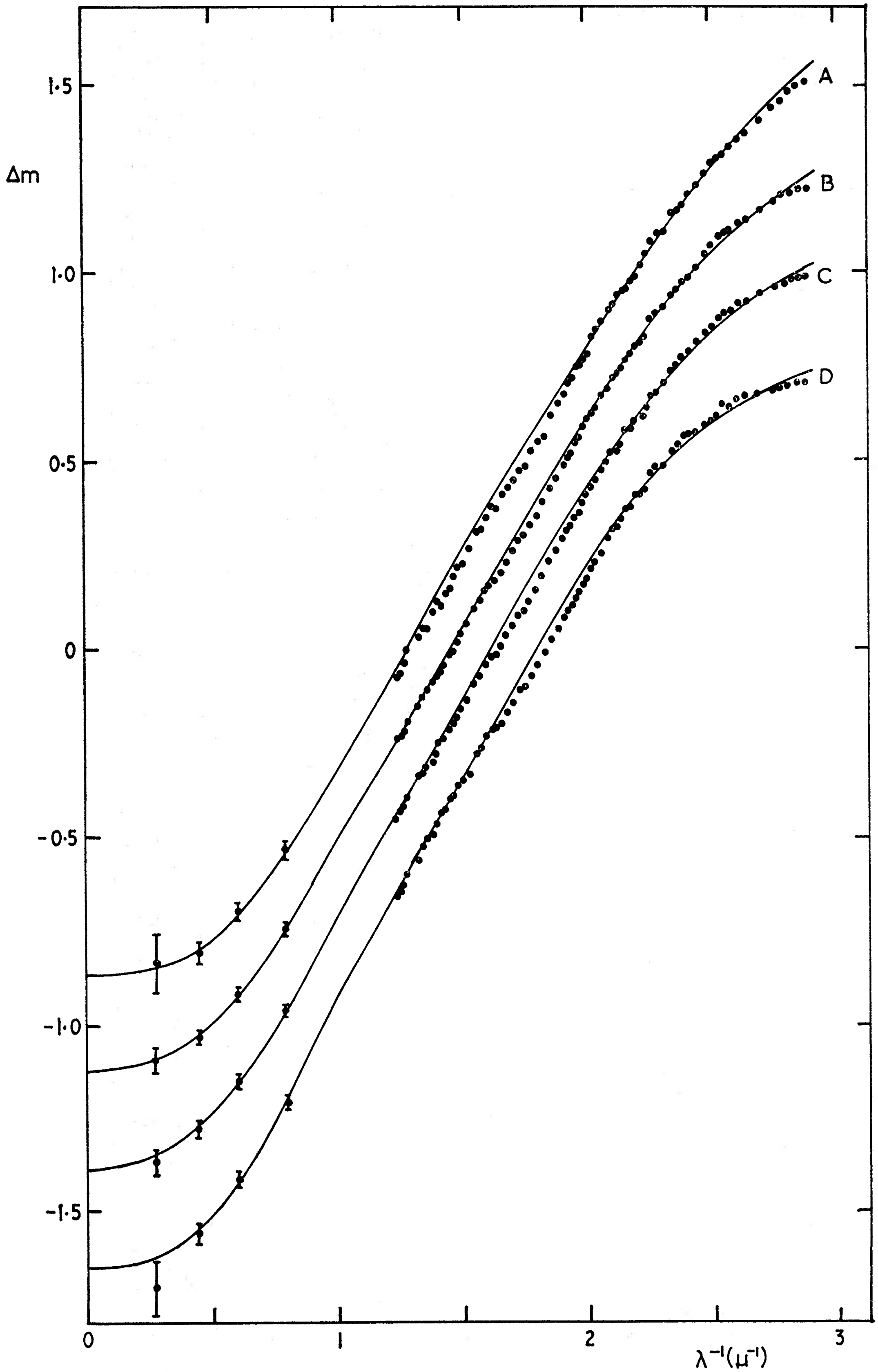

FIG. 3. *Theoretical models fitted to mean curves A, B, C and D.*

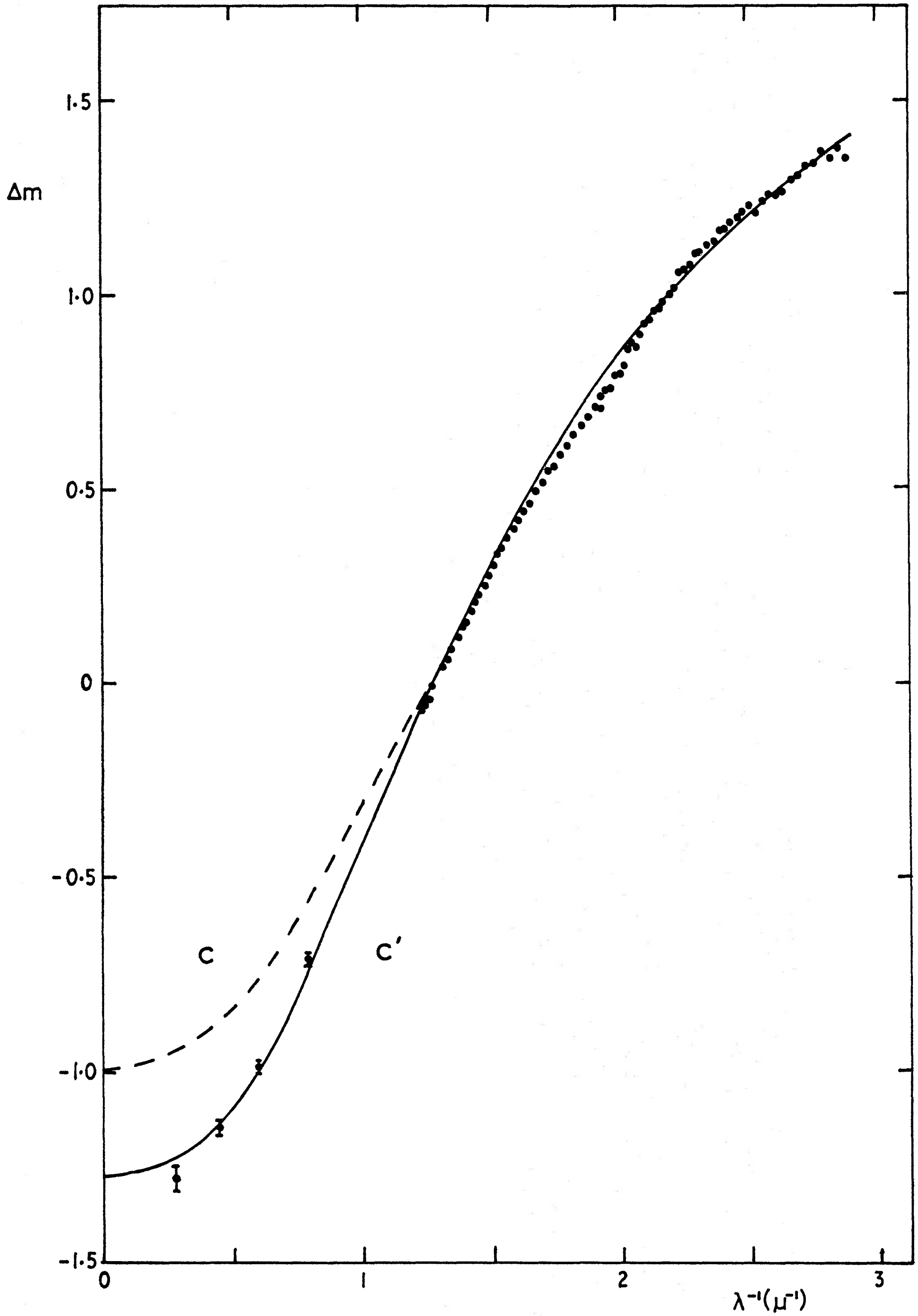

FIG. 4. *Theoretical model fitted to mean curve C′ (HD 147889). The theoretical curve C is also shown in the infrared (broken line).*

4. *R* VALUES

In order to compute *R* values we require a knowledge of the way in which the curve approaches the $\lambda^{-1} = 0$ axis. The extinction due to the iron component of the models is vanishingly small for $\lambda^{-1} < 0{\cdot}2\ \mu^{-1}$ and may be neglected. The contribution of graphite is also small in the far infrared, and any uncertainty in the optical constants has minimal effect. In the case of silicates there is structure in the optical constants which produces absorption bands at 0·11 and 0·05 μ^{-1} (see Bromage, Nandy & Khare 1973). These are superposed on the smooth curve obtained by assuming a constant value for the refractive index for $\lambda^{-1} < 0{\cdot}2\mu^{-1}$, which tends to a λ^{-4} law as the wavelength becomes very large compared with the mean grain size. The silicate infrared bands are not shown in Figs 3 and 4 because of their narrowness. The *R* values appropriate to each mean curve are given in Table IV, deduced directly from Figs 3 and 4 by measuring

$$R = \frac{\Delta m(\lambda_V^{-1}) - \Delta m(0)}{\Delta m(\lambda_B^{-1}) - \Delta m(\lambda_V^{-1})}$$

where $\lambda_B = 4400$ Å and $\lambda_V = 5530$ Å are the effective wavelengths of the *B* and *V* filters. $\Delta m(\lambda_B^{-1})$ and $\Delta m(\lambda_V^{-1})$ were measured from the observational curve and $\Delta m(0)$ from the theoretical curve. The uncertainty in the results was estimated by considering the range of theoretical curves which could be said to fit the infrared points in each case, giving limiting values of $\Delta m(0)$. The *L* data point (0·286 μ^{-1}) was ignored in the model fitting for the reasons noted in Section 1.

Table V gives *R* values and related data for the individual stars. The *R* values were deduced by means of the model giving the best fit to the extinction curve in each case (column 2), and are not always identical to the *R* values of the appro-

TABLE V

R Values and associated data for individual reddened stars

HD	*R* (±0·2)	M_V	A_V	*d* (kpc)	ΔL Se	λ_{max} (μ)
77581	3·3	−5·8	2·4	1·13	0·01±0·08	0·54
90706	3·1	−5·7	1·9	1·49	0·00±0·12	0·56
92964	3·5	−6·8	1·3	1·54	0·28±0·16	0·58
115842	3·5	−6·2	1·8	1·22	0·05±0·10	—
142468	3·2	−6·4	2·6	2·14	0·12±0·13	—
144969	3·2	−6·4	3·7	1·56	0·06±0·05	0·55
147084	3·6	(−2·7)	2·6	(0·08)	0·00±0·03	0·67
147889	4·3	−2·5	4·7	0·14	0·05±0·03	0·80
148379	3·2	−6·8	2·3	0·93	0·09±0·06	0·60
148688	3·4	−6·6	1·7	1·09	0·12±0·07	0·53
152235	3·0	−6·4	2·3	1·21	0·02±0·03	0·46
152236	3·5	−8·2	2·4	1·28	0·10±0·05	0·58
154043	3·0	−6·2	2·4	1·48	0·01±0·04	—
156201	3·0	−6·4	2·6	2·18	0·01±0·05	—
165319	3·1	−6·2	2·6	2·06	0·00±0·08	—
166628	3·0	−6·8	2·1	2·37	0·01±0·03	—
167838	3·3	−7·0	1·8	2·41	0·05±0·03	—
168571	3·1	−5·0	2·4	1·20	−0·02±0·07	0·52
169454	3·2	−8·2	3·6	1·73	0·00±0·03	0·55
170939	3·2	−6·6	3·3	1·69	0·00±0·05	0·51
171012	3·4	−6·4	2·3	1·54	0·08±0·06	—
172488	2·7	−5·2	2·2	1·36	−0·01±0·07	—

priate mean curve. Column 3 of Table V gives the absolute magnitude M_V determined from the MK spectral type using the calibration of Blaauw (1963); the visual absorption $A_V = R.E_{B-V}$ and distance d (kpc) are given in columns 4 and 5. The difference ΔL between the observational and theoretical curves at 3·4 μ is taken as a measure of the infrared excess and is listed with standard photometric errors in column 6. Positive values refer to cases where the observational curve falls below the theoretical curve. Column 7 gives the wavelength of maximum linear polarization λ_{max} (microns), where available from the data of Serkowksi, Mathewson & Ford (1975) and Coyne, Gehrels & Serkowski (1974), which is used to test for correlation with R in the following section.

5. DISCUSSION

Figs 3 and 4 illustrate that the chosen grain model is capable of producing theoretical curves which match the general shape of the observational curves fairly closely. The fits were obtained by varying the relative contributions of the small and large grain species in the model, suggesting that there are more small grains than average in the line of sight to law A and law B stars and less towards law D stars, compared with law C. In the case of HD 147889, in the ρ Oph complex, an increase in the characteristic size of the largest grain species was required to fit the curve, leading to an R value of 4·3. This may be interpreted in terms of grain growth in the dense central region of the complex, as suggested by Carrasco, Strom & Strom (1973) and discussed by Whittet & van Breda (1975). HD 147084, which lies about 1° from the cloud centre, has an R value of 3·6. The R values deduced for the remaining 20 stars in Table V lie in the range 2·7–3·5 with a median value of 3·2, thus no substantial departures from normal interstellar extinction are implied for these stars.

The computed curves do not give a precise, detailed fit to the observational data as the model cannot reproduce very broadband structure (VBS) which is present in the curves. In Paper II we noted a slight dip in the extinction for HD 92964 in the wavenumber range 1·6–1·9 μ^{-1}, and a cusp-like depression at λ^{-1} = 1·97 μ^{-1} for HD 147889. The first of these features is present to some extent in all of the curves except that for HD 147889, and in this case the cusp may be a manifestation of the same feature shifted to shorter wavelength. A 1·6–1·9 μ^{-1} dip was also noted by Whiteoak (1966) in his extinction data for Northern Milky Way stars and therefore appears to be a widespread phenomenon. Hayes *et al.* (1973) proposed a model involving impurities in the grains to explain the VBS in terms of two broad, shallow absorption bands in adjacent regions of the spectrum. Here we are concerned only with the overall properties of the extinction; we note, however, that the derived R values are lower by ~0·3 than would be the case in the absence of the VBS as the observational curve falls below the fitted theoretical curve by ~0^m·04 at the wavelength of the V band. The R value derived for HD 147084 is higher than that for the mean law C curve as the VBS is weak for this star.

It was suggested by Serkowski (1968) that R may be correlated with the wavelength of maximum linear polarization. Serkowski *et al.* (1975) present λ_{max} measurements for a large sample of stars, and note a correlation with colour

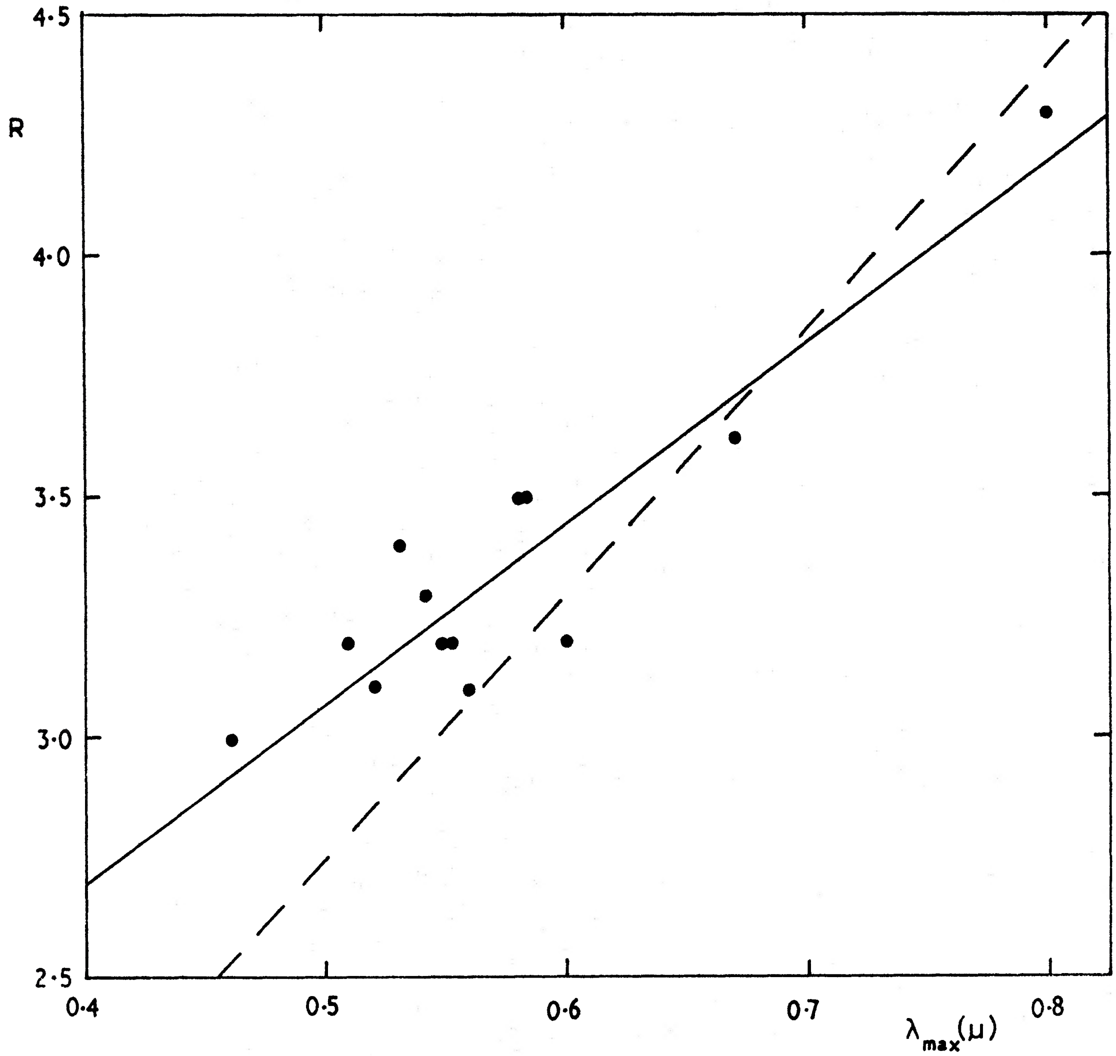

FIG. 5. *Plot of derived R values against the wavelength of maximum linear polarization for 13 stars.*

excess ratios from which they deduce the relation

$$R = 5{\cdot}5\ \lambda_{max}$$

where λ_{max} is measured in microns. This formula is based on the assumption that

$$R = 1{\cdot}1\ \frac{E_{V-K}}{E_{B-V}}$$

which holds for a normal van de Hulst theoretical curve (see Carrasco *et al.* 1973). Values of λ_{max} are available for 13 of our reddened stars, listed in column 7 of Table V. Fig. 5 shows a plot of our extinction curve R values against λ_{max}. The broken line represents the relation derived by Serkowski *et al.* (above) and the continuous line gives the best straight line fit to the points:

$$R = a\lambda_{max}+b$$

where

$$a = 3{\cdot}7 \pm 0{\cdot}6 \text{ and } b = 1{\cdot}2 \pm 0{\cdot}3.$$

The difference between these relations is only significant for stars with low λ_{max} values of which there are few in our list, and further extinction curve R value determinations for such stars would be required to establish a more precise empirical relationship between the two parameters. The importance of this correlation is that it gives a direct method of measuring R for individual stars by means of observations in the visual and near infrared regions only, without the problems involved in extrapolating the extinction curves to $\lambda^{-1} = 0$. Serkowski *et al.* used their catalogue of data to study variations in λ_{max} with position in the Galaxy, and found several well-defined regions where λ_{max}, and hence R, is systematically larger or smaller than the median value of $\bar{\lambda}_{max} = 0{\cdot}545\ \mu$ (corresponding to $R = 3{\cdot}0$ using their formula, or $3{\cdot}2$ using ours). Whittet & van Breda (1975) noted that λ_{max} is high for several stars associated with compact dark clouds or dust complexes: in particular, the polarization data confirm our R value of $4{\cdot}3$ for HD 147889 in the ρ Oph complex.

Column 5 of Table V indicates that there are 4 stars (HD 92964, 148379, 148688 and 152236) which show apparent infrared excesses ΔL at $3{\cdot}4\ \mu$ which are appreciably larger than the photometric errors. There are a further 5 stars with excesses comparable with the errors, and the remaining 13 show no significant differences between observational and theoretical curves at this wavelength. There are no stars with significant negative ΔL values. We must first consider the possibility that the effect is cause by a difference in the L band filter effective wavelength for the reddened and comparison stars. Gutierrez–Moreno & Moreno (1975) have considered this problem in *UBV* photometry: they concluded that the ratio E_{U-B}/E_{B-V} is virtually independent of reddening and that A_V/E_{B-V} varies more with spectral type than with reddening. There is no obvious correlation of the ΔL values in Table V with either spectral type or reddening. For example, HD 165319 (B0Ia) and HD 147084 (A5II) both have zero ΔL values. E_{V-L} is plotted against E_{B-V} in Fig. 6 for 27 stars for which L magnitudes are available from our observations (Tables I and II) or those of Johnson (1968). The intrinsic colours tabulated by Johnson have been used to deduce the colour excesses. In order to exclude stars with abnormal extinction curves only those with λ_{max} measures available which lie in the range $0{\cdot}5$–$0{\cdot}6\ \mu$ ($R = 3{\cdot}05$–$3{\cdot}42$ by our formula) are plotted. The straight line $E_{V-L} = 3{\cdot}05\ E_{B-V}$, which represents normal extinction with $R = 3{\cdot}2$ is drawn in Fig. 6. The four stars with significant ΔL values (labelled) lie slightly above this line. There is no evidence for marked deviation from linearity in the plot at high E_{B-V} which could arise from change in the L band filter effective wavelength with reddening. It is probable that the small excesses measured for the four labelled stars result from free–free emission in the stellar atmospheres (see Dyke & Milkey 1972), an interpretation which is supported by the fact that they are all type Ia supergiants and probably have gaseous envelopes due to mass loss (Jaschek & Brandi 1973; Jaschek & Jaschek 1973; Hutchings 1976). Woolf, Stein & Strittmatter (1970) concluded that free–free emission is a more likely source of infrared excess in Be stars than radiation from circumstellar dust shells. The lack of evidence for infrared emission from circumstellar grains does not rule out the possibility that the stars have ‘ local ’ components to their extinctions in which the grain size distribution may be modified by radiation from the star itself, as indicated in Paper I. HD 147084 and HD 147889 are almost certainly imbedded in the dust complex producing their extinctions, but local dust is in general unlikely to produce measurable thermal emission at $3{\cdot}4\ \mu$. Thus deter-

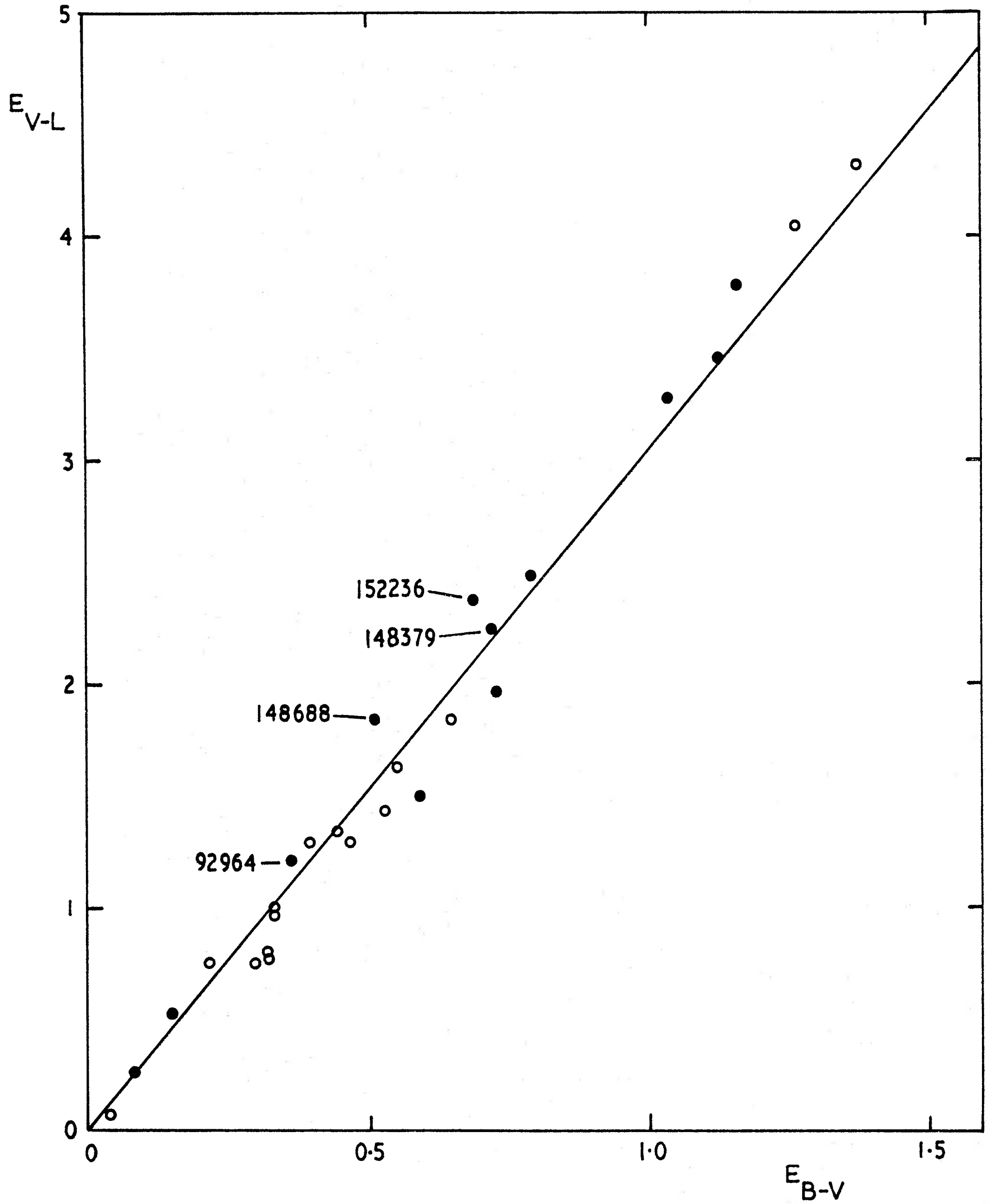

FIG. 6. *Plot of E_{V-L} against E_{B-V} for 27 stars. The straight line represents normal extinction (E_{V-L} = 3·05 E_{B-V}).*

mination of the scale of 'local' variations in the properties of the dust must be achieved by alternative means such as the comparison of the extinction curves of stars close to each other in the sky.

Fig. 7 shows the positions of the reddened stars projected on to the galactic plane. The boundaries of the spiral arms are taken from Nandy (1965), and the stars are labelled 1–22 in order of increasing HD number. Most of the observed stars are situated within or on the near boundary of the Carina–Sagittarius arm. Nandy (1965) found significant differences between the mean extinction laws for Cygnus and for Perseus stars which suggests a possible systematic variation with line of sight relative to the local spiral arm, as predicted by Greenberg & Meltzer (1960) and by Wilson (1960). The extinction curve A (HD 172488, star no. 22,

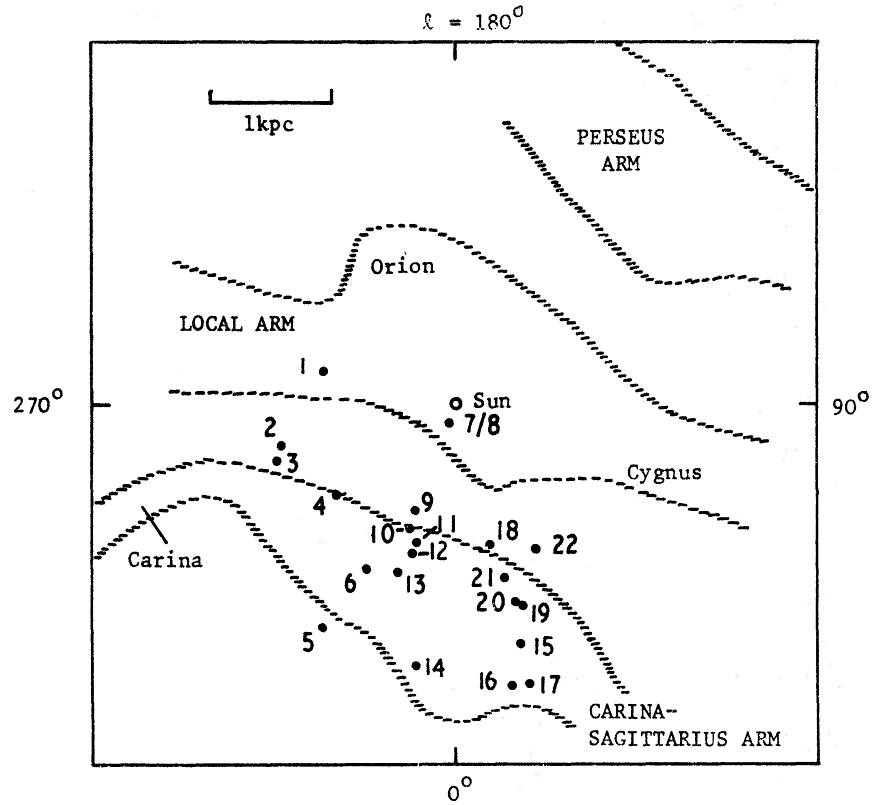

FIG. 7. *Positions of the reddened stars projected on to the galactic plane. Boundaries of the spiral arms are taken from Nandy* (1965). *The stars are labelled* 1–22 *in order of increasing HD number.*

Fig. 7) is very similar to Nandy's curve for Cygnus: in both cases the extinction in the near ultraviolet is higher than average. HD 172488 is the most northerly star in our list, situated 30° along the Milky Way from Cygnus. The mean extinction curve for low latitude stars in the longitude interval $l = 330°–0–20°$ (i.e. roughly perpendicular to the local arm, opposite to Perseus) is close to law C, which is very similar to Nandy's Perseus curve. Thus, despite the variations from star to star, our results are not inconsistent with an underlying systematic variation between Cygnus (law A) and Perseus (law C) extinction with l, bearing in mind that regional fluctuations in the mean grain size may slightly modify the curve for individual stars. The systematic effect would produce a variation in R of 2·7–3·3, and thus blanket application of $R = 3·0$ in photometric distance determinations will not lead to any major misconstruction of spiral structure. We find no support in our results for the suggestion of Crézé (1972) that R varies between 4·0 and 1·5 according to the proportion of the line of sight lying within spiral arms.

The line of sight to HD 77581 (star no. 1, Fig. 7), which is a spectroscopic binary associated with Vel X-1, lies completely within the local spiral arm in the opposite direction to Cygnus. The ratio of visual absorption to distance is 2·1 mag kpc^{-1} for this star, compared with a weighted mean of 1·5 mag kpc^{-1} for the remainder with long-path-length reddening. We detect no significant infrared excess for HD 77581 and conclude that its extinction law and spectral energy distribution are unexceptional (apart from stronger than average broadband structure), in agreement with the results of Hyland & Mould (1973).

The stars HD 90706 and HD 92964 (nos 2 and 3, Fig. 7) are intermediate in distance between the Sun and the η Carinae complex. Their reddening probably arises largely in a diffuse dark cloud at a distance of ~0·8 kpc from the Sun (see Graham 1971). HD 90706 is a member of the open cluster IC 2581 (Lloyd Evans 1969) which is associated with nebulosity. There has been some controversy recently over the value of R appropriate to this cluster. Turner (1973) deduced $R \sim 5{\cdot}5$ by the variable extinction method, a result which is disputed by Moffat (1974). Turner (1976) has reasserted that the extinction is anomalous in this region. Turner's values for R and the cluster distance imply that $M_V \sim -7{\cdot}5$ for HD 90706, which is inconsistent with the spectral classification given by Lloyd Evans. The extinction curve we have obtained for this star is not unusual, yielding an R value of $3{\cdot}1 \pm 0{\cdot}2$; it also has a normal value of λ_{max} (Table V).

He 152235 and HD 152236 (nos 11 and 12, Fig. 7) are regarded as probable members of the Sco OB 1 association (Schild, Hiltner & Sanduleak 1969). However, the distances derived for these stars in Table V (~1·3 kpc) are much less than the value of $2{\cdot}4 \pm 0{\cdot}2$ deduced for the association by Schild, Neugebauer & Westphal (1971) on the assumption that $R = 3$. As this assumption appears to be reasonable in this case, it must be concluded that either the stars are foreground to the association or the absolute magnitudes used are too faint by $\sim 1^{m}{\cdot}5$. A similar problem arises for HD 147084, as discussed by Whittet (1974). This star is a probable member of Sco OB 2; if its distance is taken to be 170 pc, as determined kinematically by Bertiau (1958), then the value of A_V given in Table V implies that the absolute magnitude should be $-4{\cdot}1$, compared with $-2{\cdot}7$ given by the Blaauw calibration for an A5II star.

We note in conclusion that R has now been measured for stars in the denser regions of the ρ Ophiuchi dark cloud by four independent methods, listed in Table VI. The variable extinction result applies to stars associated with emission

Table VI

Comparison of R values deduced for stars in the ρ Ophiuchi Complex by four independent methods

R	Sample	Method	Reference
$4{\cdot}2 \pm 0{\cdot}5$	14 stars in nebulosity	Variable extinction	Whittet (1974)
$4{\cdot}3 \pm 0{\cdot}2$	HD 147889	Colour difference	Paper II/ this paper
$4{\cdot}4 \pm 0{\cdot}2$	HD 147889, SR3	Polarization (λ_{max})	Whittet & van Breda (1975)
4·1	S1	Ionization of H II region	Brown & Zuckerman (1975)

Note:

SR3 is source 3 of Struve & Rudkjobing 1949; S1 is source 1 of Grasdalen, Strom & Strom 1973.

and reflection nebulosity, including HD 147889, stars not in nebulosity exhibiting a lower R value. The method of Brown & Zuckerman (1975) depends on estimating the luminosity of the star from the extent of ionization in the nearby H II region, and uses an assumed distance for the complex.

ACKNOWLEDGMENTS

We are indebted to the Large Telescope Users' Panel and to the Director Cerro Tololo Interamerican Observatory for the allocation of observing time, and to the Science Research Council for financial support.

REFERENCES

Aannestad, P. A. & Purcell, E. M., 1973. *A. Rev. Astr. Astrophys.*, **11**, 309.
Bertiau, F. C., 1958. *Astrophys. J.*, **128**, 533.
Blaauw, A., 1963. *Basic astronomical data*, p. 383, ed. K. Aa. Strand, University of Chicago Press.
Blanco, V. M., Demers, S., Douglass, G. G. & FitzGerald, M. P., 1968. *Publ. US Naval Obs.*, **21**.
Bless, R. C. & Savage, B. D., 1972. *Astrophys. J.*, **171**, 293.
Bromage, G. E., Nandy, K. & Khare, B. N., 1973. *Astrophys. Space Sci.*, **20**, 213.
Brown, R. L. & Zuckerman, B., 1975. *Astrophys. J.*, **202**, L125.
Buscombe, W., 1969. *Mon. Not. R. astr. Soc.*, **144**, 1.
Carrasco, L., Strom, S. E. & Strom, K. M., 1973. *Astrophys. J.*, **182**, 95.
Cousins, A. W. J., 1973. *Mon. Notes astr. Soc. sth. Afr.*, **32**, 117.
Coyne, G. V., Gehrels, T. & Serkowski, K., 1974. *Astr. J.*, **79**, 581.
Crézé, M., 1972. *Astr. Astrophys.*, **21**, 85.
Divan, L., 1971. *Astr. Astrophys.*, **12**, 76.
Dyke, H. M. & Milkey, R. W., 1972. *Publ. astr. Soc. Pacific.*, **84**, 597.
Glass, I. S., 1973. *Mon. Not. R. astr. Soc.*, **164**, 155.
Glass, I. S., 1974. *Mon. Notes astr. Soc. sth. Afr.*, **33**, 53.
Graham, J. A., 1971. *Dark nebulae, globules and protostars*, p. 27, ed. B. T. Lynds, University of Arizona Press.
Grasdalen, G. L., Strom, K. M. & Strom, S. E., 1973. *Astrophys. J.*, **184**, L 53.
Greenberg, J. M., 1973. *Molecules in the galactic environment*, p. 93, John Wiley & Sons, New York.
Greenberg, J. M. & Meltzer, A. S., 1960. *Astrophys. J.*, **132**, 667.
Gutierrez-Moreno, A., & Moreno, H., 1975. *Publ. astr. Soc. Pacific*, **87**, 425.
Hayes, D. S., Mavko, G. E., Radick, R. R., Rex, K. N. & Greenberg, J. M., 1973. *IAU Symp.*, **52**, p. 83, D. Reidel Publ. Co., Dordrecht.
Hutchings, J. B., 1976. *Astrophys. J.*, **203**, 438.
Hyland, A. R. & Mould, J. R., 1973. *Astrophys. J.*, **186**, 993.
Jaschek, C., Conde, H. & de Sierra, A. C., 1964. *Catalogue of MK spectral classifications*, University of La Plata, Argentine.
Jaschek, M. & Brandi, E., 1973. *Publ. astr. Soc. Pacific*, **85**, 736.
Jaschek, M. & Jaschek, C., 1973. *Publ. astr. Soc. Pacific*, **85**, 127.
Johnson, H. L., 1968. *Nebulae and interstellar matter*, p. 167, eds B. M. Middlehurst & L. H. Aller, University of Chicago Press.
Kennedy, P. M. & Buscombe, W., 1974. *MK spectral classifications* (published since Jaschek's La Plata Catalogue), Evanston.
Lenham, A. P. & Treherne, D. M., 1966. *Optical properties and electronic structure of metals and alloys*, p. 196, ed. F. Abeles, North Holland, Amsterdam.
Lloyd Evans, T., 1969. *Mon. Not. R. astr. Soc.*, **146**, 101.
Moffat, A. F. J., 1974. *Astr. Astrophys.*, **32**, 103.
Nandy, K., 1965. *Nature*, **208**, 274.
Nandy, K. & Wickramasinghe, N. C., 1971. *Mon. Not. R. astr. Soc.*, **154**, 255.
Pollack, J. B., Toon, O. B. & Khare, B. N., 1973. *Icarus*, **19**, 372.
Schild, R., Hiltner, W. A. & Sanduleak, N., 1969. *Astrophys. J.*, **156**, 609.
Schild, R., Neugebauer, G. & Westphal, J. A., 1971. *Astr. J.*, **76**, 237.
Serkowski, K., 1968. *Astrophys. J.*, **154**, 115.
Serkowski, K., Mathewson, D. S. & Ford, V. L., 1975. *Astrophys. J.*, **196**, 261.
Struve, O. & Rudkjobing, M., 1949. *Astrophys. J.*, **109**, 92.
Taft, E. A. & Philipp, H. R., 1965. *Phys. Rev.*, **138**, A197.
Turner, D. G., 1973. *Astr. J.*, **78**, 597.
Turner, D. G., 1976. *Astr. J.*, **81**, 97.
van Breda, I. G., Glass, I. S. & Whittet, D. C. B., 1974. *Mon. Not. R. astr. Soc.*, **168**, 551. Paper II.
Whiteoak, J. B., 1966. *Astrophys. J.*, **144**, 305.
Whittet, D. C. B., 1974. *Mon. Not. R. astr. Soc.*, **168**, 371.

Whittet, D. C. B., Dayawansa, I. J., Dickinson, P. M., Marsden, J. P. & Thomas, B., 1976. *Mon. Not. R. astr. Soc.*, **175**, 197.
Whittet, D. C. B. & van Breda, I. G., 1975. *Astrophys. Space Sci.*, **38**, L3.
Whittet, D. C. B., van Breda, I. G. & Nandy, K., 1973. *Nature Phys. Sci.*, **243**, 21. Paper I.
Wickramasinghe, N. C., 1967. *Interstellar grains*, p. 10, Chapman & Hall.
Wickramasinghe, N. C., 1974. *Nature*, **252**, 468.
Wickramasinghe, N. C., 1975. *Mon. Not. R. astr. Soc.*, **170**, 11P.
Wickramasinghe, N. C. & Nandy, K., 1970. *Nature*, **227**, 51.
Wickramasinghe, N. C. & Nandy, K., 1971. *Mon. Not. R. astr. Soc.*, **153**, 205. (WN in text.)
Wilson, R., 1960. *Mon. Not. R. astr. Soc.*, **120**, 51.
Woolf, N. J., Stein, W. A. & Strittmatter, P. A., 1970. *Astr. Astrophys.*, **9**, 252.